ChemCatChem

Research Article
doi.org/10.1002/cctc.202200268

Chemistry Europe
European Chemical Societies Publishing

www.chemcatchem.org

One-pot Synthesis of Hierarchical, Micro-macroporous Zeolites with Encapsulated Metal Particles as Sinter-resistant, Bifunctional Catalysts

Tobias Weissenberger,*[a] Nidhi Kapil,[a] Panagiotis Trogadas,[a] and Marc-Olivier Coppens*[a]

We report a new one-pot synthesis procedure for hierarchical zeolites with intracrystalline macropores and metal particles encapsulated within the zeolitic walls. The synthesis allows to prepare macroporous zeolites of MFI topology with different heteroatoms (silicalite-1, ZSM-5 and TS-1) and different encapsulated noble metal particles, such as gold, platinum and palladium. The hierarchically structured zeolites contain large macropores with diameters around 400 nm, which are well distributed and interconnected and should significantly enhance mass transport properties. The encapsulation of metal nanoparticles within the zeolitic walls leads to remarkable sinter resistance of the particles. Encapsulated gold nanoparticles (2.6 nm) do not significantly change in size during an 18-hour treatment at 600 °C under air, while non-encapsulated gold particles sinter heavily during the same treatment. Catalytic experiments for the direct epoxidation of propene with hydrogen and oxygen show that both catalytic functions of a macroporous TS-1 sample that encapsulates gold particles are accessible and active. This catalyst displays high activity, although PO selectivity could still be improved. These materials show great potential for use in catalytic applications, due to their bifunctional nature, high sintering resistance, shape selective properties and hierarchical structure.

Introduction

Noble metals, such as gold, platinum, palladium or ruthenium, are among the most important catalytic materials, because of their remarkable performance to catalyse a wide range of reactions relevant in the chemical industry, energy conversion, and environmental protection.[1] Especially nanosized noble metal particles are effective catalysts, due to their high surface area to volume ratio and large number of active facets.[2]

For catalytic applications, noble metals are commonly used as small particles dispersed on a porous support material, such as alumina, silica, titania, zeolites or carbon materials.[3] The support provides a large surface area necessary to disperse the metal particles and thus reach a higher utilisation.

Despite much progress in material design, sintering is still an inherent limitation of noble metal catalysts.[4] During catalytic applications, especially at higher temperatures, metal nanoparticles are subject to sintering and aggregation to form larger particles and thus minimise their surface energies.[5] The formation of larger particles and the subsequent loss of available metal surface for catalysis results in irreversible catalyst deactivation. Considering the high cost for metal catalysts, especially the widely applied noble metals, this irreversible catalyst deactivation is an economic and environmental problem in industrial catalysis.

One way to prevent sintering of metal particles is the encapsulation within a porous matrix. The metal particles become only accessible by diffusion through the pores and are separated from each other by the walls of the porous matrix, which prevents the particles to sinter and aggregate.[6]

Beside the typical demands for a catalyst support, the porous matrix material must feature a small enough pore size to avoid sintering by transport through the pores, which are usually smaller than the metal particle size. Mesopores are often already too large and metals can sinter within the mesopores.[7] One class of materials suitable for this are zeolites. These inorganic, crystalline materials possess high thermal stability and a well-defined micropore system, with pore diameters usually in the range of 0.35 to 1 nm, making them ideal for the prevention of sintering of encapsulated metal particles.[1a,8] Furthermore, depending on the type of heteroatoms and counter ions, zeolites can provide different active sites (such as Brønsted or Lewis acidic and basic sites)[9] to be used as multifunctional catalysts for tandem catalysis.[10] The zeolites also provide the catalysts with unique shape selectivity via the micropore network, since the metal particles are encapsulated, and thus only accessible via the micropores.[11] This allows, for example, shape selective hydrogenation on encapsulated Pt or Pd particles.[11a,12]

However, the diffusion of molecules to the active sites located in a zeolite crystal (both the zeolitic acid sites and the

[a] Dr. T. Weissenberger, Dr. N. Kapil, Dr. P. Trogadas, Prof. M.-O. Coppens
Centre for Nature Inspired Engineering, Department of Chemical Engineering
University College London
Torrington Place
London, WC1E 7JE (UK)
E-mail: tobias.weissenberger@imm.fraunhofer.de
m.coppens@ucl.ac.uk

Supporting information for this article is available on the WWW under https://doi.org/10.1002/cctc.202200268

encapsulated metal particles) is very slow due to the tightness with which many molecules are confined within the pores. This can lead to severe diffusion limitations.[13] These diffusion limitations often result in reduced utilisation of the zeolite crystal and can also lead to a lower selectivity or catalyst lifetime. Hierarchical zeolites, consisting of at least one additional system of larger pores interconnected to the zeolitic micropores, could already demonstrate enhanced diffusion properties and, consequently, better catalytic performance, compared to conventional, purely microporous zeolites in several test reactions.[14]

To this day, no reports of macroporous zeolites with encapsulated metal particles can be found in the literature. Such a bifunctional catalyst has the potential to be very beneficial for many different reactions, which encounter problems like diffusion limitations or sintering of the metal particles.

In this paper, we introduce a one-pot synthesis route for hierarchical macro-microporous zeolites with encapsulated noble metal nanoparticles. For this novel synthesis route, combining the steam-assisted crystallisation of mesoporous silica particles (MSPs)[15] with the addition of stabilised metal precursors, a new impregnation procedure was developed. Firstly, the MSPs were impregnated with the titanium source in a wet impregnation step to allow even distribution over the MSPs. After drying, an incipient wetness impregnation step followed by fast drying was used to add the structure-directing agent and noble metal precursors.

For the stabilisation of the noble metal precursors, 3-mercaptopropyl-trimethoxysilane was used, which was previously reported by Iglesia and co-workers to effectively stabilise metal precursors during hydrothermal synthesis.[16]

Results and Discussion

Textural and physicochemical analysis of Au/MTS-1

Characterisation results for a representative sample of Au/MTS-1 are shown in Figure 1. The XRD pattern of the calcined sample shows the typical refraction lines for MFI, without visible phase impurities. The N_2 adsorption/desorption isotherms, shown in Figure 1f, represents a IUPAC Type 1 isotherm, which is typical for a microporous material. The values for the BET surface area (431 $m^2 g^{-1}$) and the micropore volume (0.17 $cm^3 g^{-1}$) are also typical for a highly crystalline MFI zeolite.

The calcination treatment, necessary to remove the structure directing agent from the micropores of the zeolite, usually results in sintering of the metal particles. However, this is not the case for the Au/MTS-1 sample. The TEM micrographs of Au/MTS-1 (a) before and (b) after calcination at 823 K are compared in Figure 1(a–c). The zeolite crystals are around 3 μm in size and show well defined macropores with a diameter around 450 nm;

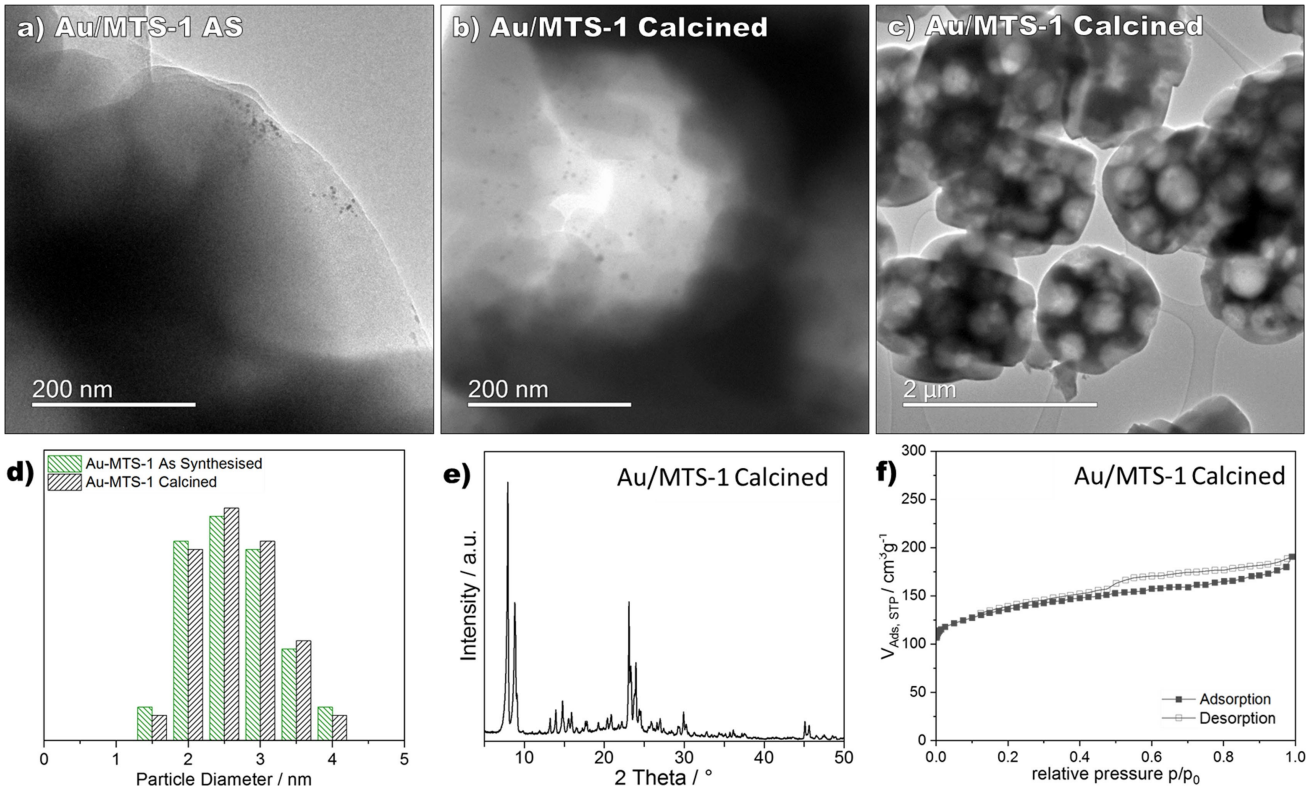

Figure 1. a–c) TEM images of the as-synthesised (AS) and calcined Au/MTS-1 samples; d) particle size distribution of the encapsulated gold particles before and after calcination, where particle sizes were estimated by measuring 200 particles in the TEM images; e) PXRD pattern and f) nitrogen adsorption and desorption isotherms of the calcined Au/MTS-1 sample.

as expected, these sizes are not affected by the calcination treatment. The macropores appear to be interconnected and are evenly distributed over all crystals. This is in good agreement with earlier work that demonstrated the high interconnectivity between the macropores by using electron and ptychographic X-ray tomography techniques.[15b,17] This hierarchical pore network drastically reduces the diffusion path lengths within the microporous domains and, combined with substantially higher diffusion rates in the macropores, should enhance the overall mass transport compared to conventional zeolites, as long as the additional interfaces do not create surface barriers.[14c,18]

The Au nanoparticles are only present in the crystals: no "free" Au nanoparticles were visible. Furthermore, the nanoparticles are homogenously distributed over the crystals with an average particle diameter of 2.6 nm. After the harsh calcination treatment, no change in the particle diameter is evident in the data. Since a high temperature would usually result in severe sintering of supported gold particles, the retained particle size is a clear indication that the particles are encapsulated within the zeolite framework. Elemental analysis of the calcined sample showed a gold loading of 0.97 wt%, which is close to the 1.0 wt% added to the synthesis mixture, indicating almost no gold loss during synthesis. The Si/Ti ratio of 63 is also close to the set value of 60, demonstrating a high utilisation of the added titanium source.

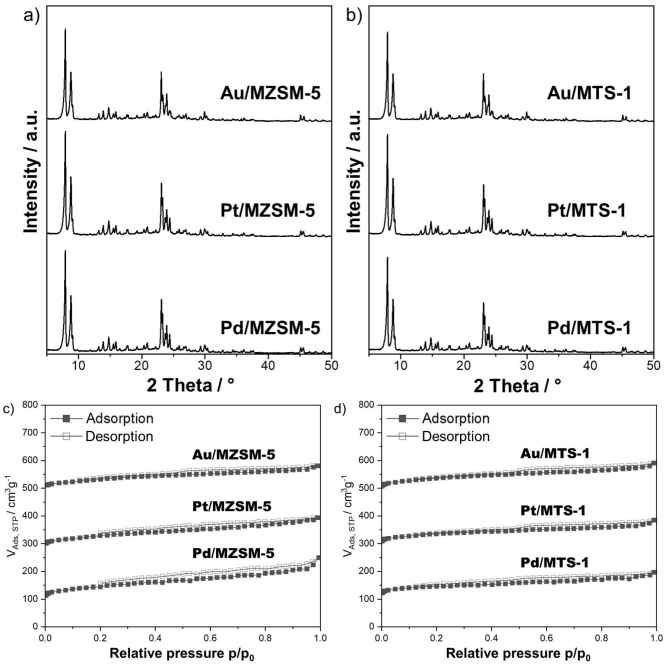

Figure 2. Powder XRD patterns of the calcined hierarchical a) MZSM-5 and b) MTS-1 zeolites with different encapsulated noble metals. Nitrogen adsorption and desorption isotherms of the calcined hierarchical c) MZSM-5 and d) MTS-1 zeolites with different encapsulated noble metals.

Au, Pt and Pd encapsulated in MZSM-5 and MTS-1 zeolites

To cover a wide range of catalytic applications, a set of samples with different noble metals and heteroatoms was synthesised, and the calcined samples were analysed. The powder XRD patterns, shown in Figure 2 for MZSM-5 and MTS-1 zeolites, reveal that all synthesised samples are highly crystalline MFI zeolites without any phase impurities. The relative crystallinity of the samples estimated by integration of the MFI typical peak areas appears to be similar for all synthesised samples. The absence of Pd, Au and Pt reflections indicates that no large metal crystallites are present in the samples (e.g. Au(111) reflection would be at $2\theta = 36°$, Pt(111) at $2\theta = 39°$ and Pd(111) at $2\theta = 40°$).

The nitrogen adsorption and desorption isotherms in Figure 2c and d further confirm the high zeolitic character of the samples. All isotherms are IUPAC Type 1, characteristic for microporous materials. The micropore volumes, surface areas and total pore volumes are listed in Table ESI-1 and are typical for MFI type zeolites of high crystallinity. In good agreement with the XRD data, this shows that the addition of the noble metal and stabilisation agent did not hinder the zeolite formation during steam-assisted crystallisation, which could cause reduced crystallinity or formation of impurities.

The UV-Vis spectra of the MTS-1 samples show characteristic peaks that demonstrate the incorporation of titanium into the zeolite framework (see Figure 3). The peaks at around 205 to 210 nm can be attributed to isolated tetrahedral titanium species ($Ti(OSi)_4$) and the peak at 228 nm to titanol species

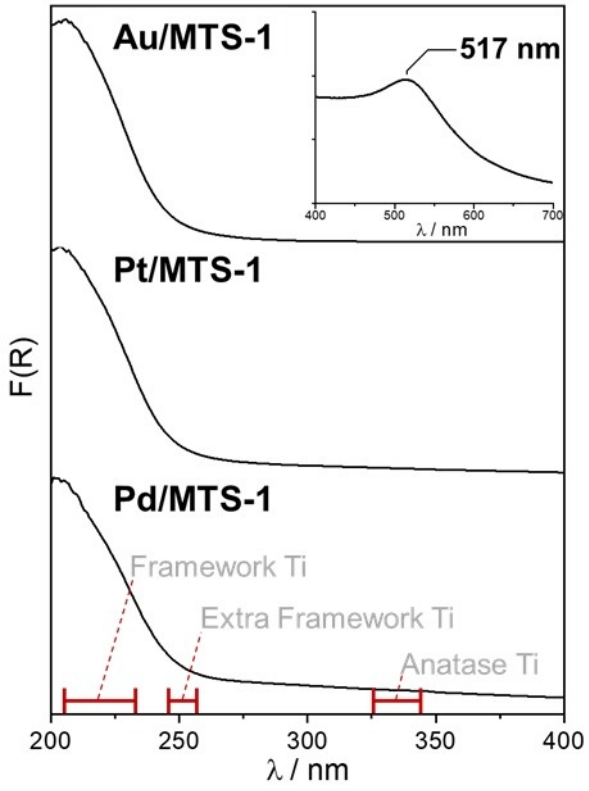

Figure 3. UV-Vis spectra of calcined MTS-1 zeolites with different encapsulated noble metals. Inlay shows the Au plasmon resonance peak for Au/MTS-1 at higher magnification.

($Ti(OH)(OSi)_2$), both incorporated into the zeolite framework. Beside framework Ti, the samples contain a small amount of extra-framework titanium species (TiO_6 isolated), visible as a broad shoulder from 240 to 260 nm in the UV-Vis spectra. Crystalline anatase TiO_2 species in the range of 325 to 340 nm cannot be found in any of the spectra.[19]

The surface plasmon resonance of Au nanoparticles is also visible in the UV-Vis spectra of Au/MTS-1 at a wavelength of 517 nm (see Figure 3, inlay at the top) and is proof for the presence of small Au nanoparticles in this sample.[20]

TEM micrographs, in Figure 4, show the synthesised and calcined, noble-metal containing MZSM-5 zeolites and the corresponding particle size distribution of the metal particles. All samples show zeolite crystals with dimensions around 2 μm and macropores between 350 and 500 nm. The gold particles with an average particle diameter of 2.4 nm are smaller than the Pt and Pd particles with average particle diameters of 5.1 and 4.9 nm, respectively.

All noble metals appear to be evenly distributed over the crystals and no metal particles outside of the crystals are visible in the TEM images. The formation of small particles within the zeolite crystals is a good indication that the stabilisation of the metal precursors by 3-mercaptopropyl-trimethoxysilane also works under steam-assisted crystallisation conditions.

The TEM images in Figure 4 of the MTS-1 samples with different noble metal particles show larger zeolite crystals with dimensions around 3 μm. The macropores have diameters ranging from 250 to 500 nm, like the ZSM-5 samples. However, the zeolitic walls appear to be thicker and, thus, the crystals are likely to have a reduced macroporosity compared to the ZSM-5 samples. The average particle diameters of the metal particles follow the same trend as observed for the ZSM-5 samples. Gold is present as the smallest particles (2.6 nm), while Pt (4.3 nm) and Pd (3.6 nm) appears as slightly larger particles.

Investigations of the sintering behaviour

Sintering of noble metal particles, especially Au, poses a major problem in catalysis, due to the loss of active surface area and the high cost of the metals. Resistance to sintering of encapsulated Au particles was investigated and compared to a conventional, supported Au/TS-1 catalyst, prepared by the deposition precipitation (DP) method. The investigations were carried out by heating the samples to 873 K for 18 h in air, followed by characterisation of the treated samples using TEM, UV-Vis and XPS.

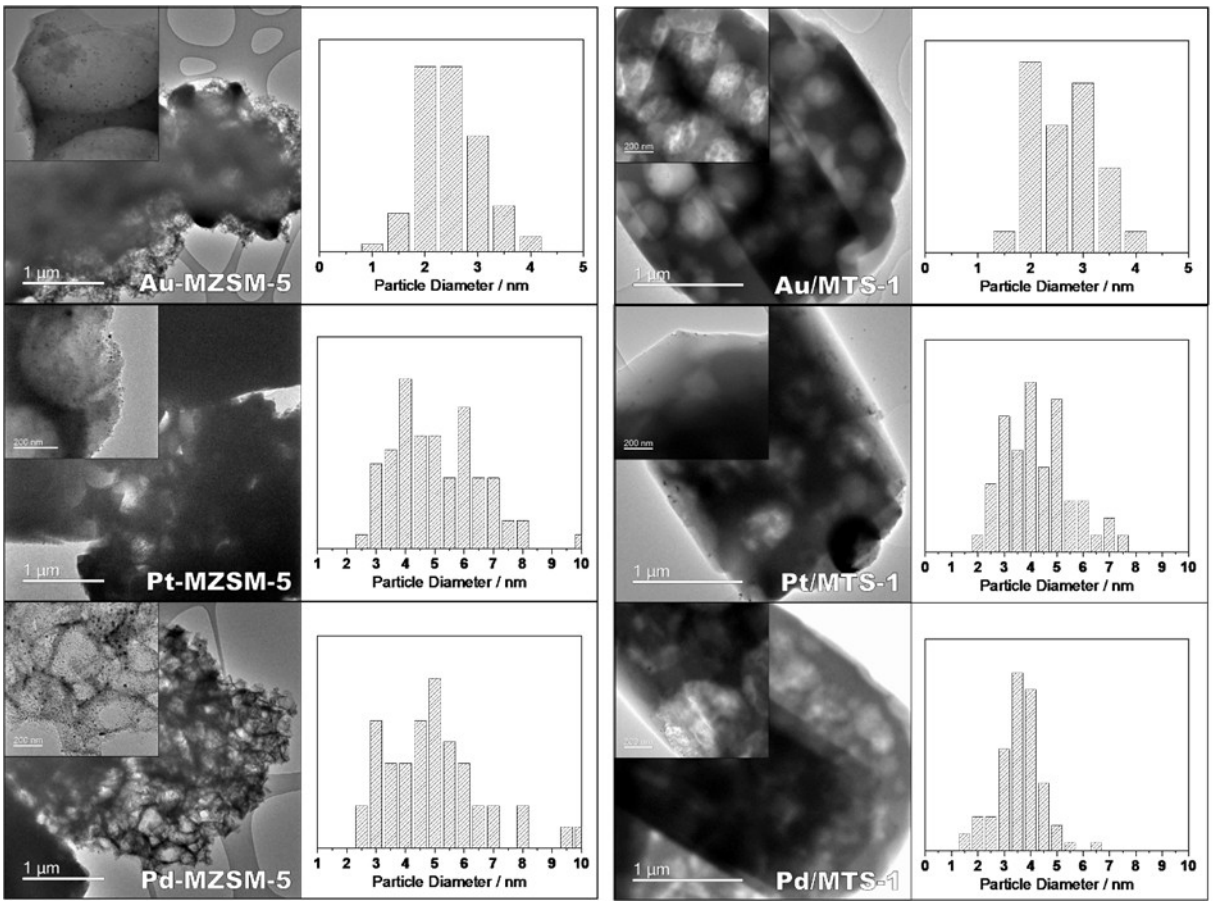

Figure 4. TEM micrographs and particle size distribution of the encapsulated noble metal in hierarchical MZSM-5 and MTS-1 zeolites with different encapsulated noble metals. Particle sizes were estimated by measuring 200 particles in the TEM images, red markers indicate metal particles.

TEM micrographs of fresh Au particles supported on TS-1, prepared by the DP method reveal an average particle diameter of 3.54 nm (Figure 5a). After the thermal treatment, the average particle diameter increased to 13.75 nm (Figure 5b and c). This is also visible in the UV-Vis spectra of the samples shown in Figure 6a: the maximum of the surface plasmon resonance peak shifts to a slightly higher wavelength, namely from 519 to 525 nm, indicating an increased particle size.

On the other hand, the sample with encapsulated gold particles shows no significant change in particle size after the same thermal treatment, as evident in the TEM images shown in Figure 5e. The freshly calcined Au/MTS-1 sample shows an average particle diameter of 2.65 nm, which increases insignificantly, to 2.70 nm, during thermal treatment.

The UV-Vis spectra of the Au/MTS-1 samples are in good agreement with the TEM data. Here, only a marginal upward shift in wavelength from 517 to 522 nm is evident in the surface plasmon resonance after the thermal treatment (Figure 6b).

X-ray photoelectron spectroscopy (XPS) was employed to investigate changes in the chemical state and size of gold clusters,[21] since the $4f_{7/2}$ orbital of gold provides a sensitive measure of its electronic state[21b] and the full-width-half-maximum (FWHM) of the gold peak is related to its particle size.[21b] Even though both Au/TS-1 samples before and after calcination contain metallic gold (Au^0), the decrease of the FWHM value of the thermally treated sample (Table 1 ESI) demonstrates the agglomeration of Au clusters,[21b] as also evidenced in the TEM micrographs (Figure 5b). In the case of the encapsulated Au/MTS-1 samples, Au is in its metallic state and the difference in FWHM is negligible (Figure 6e).

In addition, the Au $4f_{7/2}$ binding energies of all samples are shifted to lower values (~83.4 eV) compared to pure metallic Au $4f_{7/2}$ (84 eV),[22] suggesting particle-support interaction associated with electron transfer from the defect sites around TiO_x within MTS-1 to Au atoms.[23] Au is strongly adsorbed onto the oxygen vacancies of TiO_x, since the excess electron density of these sites is donated to Au atoms,[24] increasing the stability of Au/TS-1 and Au/MTS-1 catalysts.[22b,d,e] In summary, the investigations revealed that the encapsulation of gold nano particles within the hierarchical zeolites effectively prevents the sintering of the gold particles even during long treatment at high temperatures and could therefore minimise catalyst deactivation. Using a heteroatom-free, and thus inactive zeolite, such as silicalite-1, widens the possible applications to conventional mono-functional noble metal catalysts such as automotive converters since the enhanced sinter resistance provided by the zeolite could drastically reduce deactivation. An example for a sample of platinum particles encapsulated in macroporous silicalite-1 can be found in the supporting information.

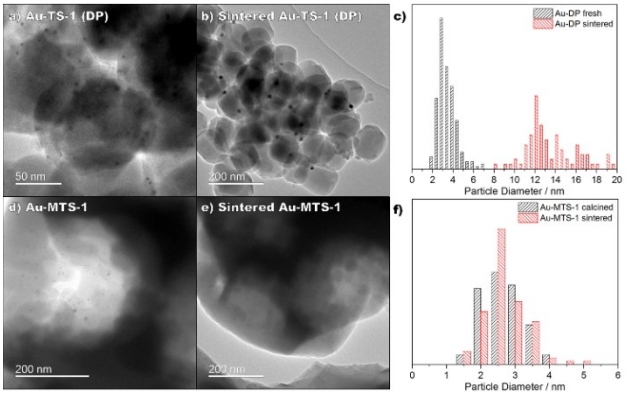

Figure 5. a–c) TEM micrographs and particle size distribution of fresh and thermally treated (873 K, 18 h) Au/TS-1 samples prepared by deposition-precipitation method (Au/TS-1 (DP)), d–f) TEM micrographs and particle size distribution of calcined and thermally treated (873 K, 18 h) Au encapsulated in macroporous TS-1 (Au/MTS-1) sample. Particle sizes were estimated by measuring 200 particles in the TEM images.

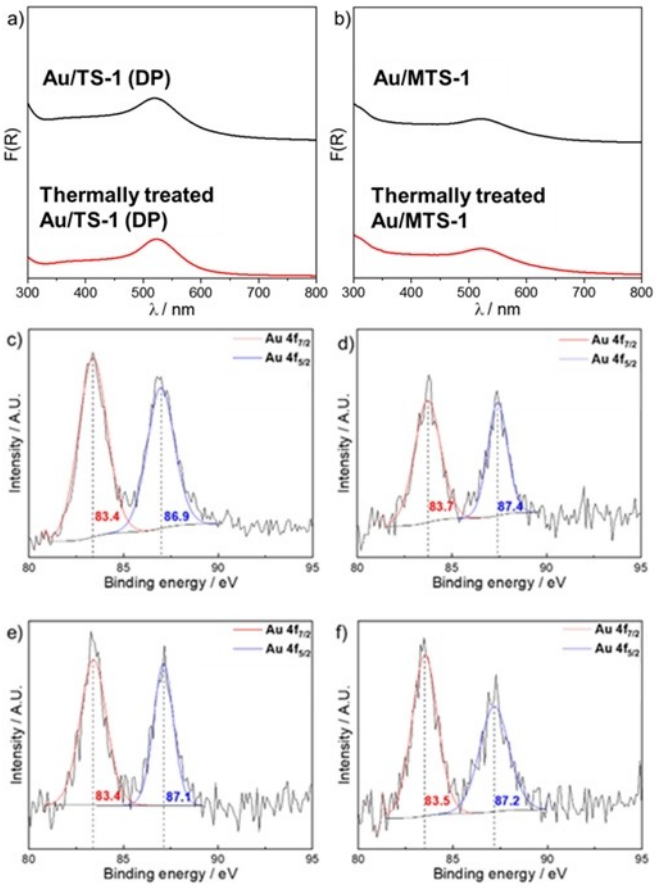

Figure 6. a) UV-Vis spectra, c) and e) XPS spectra of fresh and thermally treated (873 K, 16 h) Au/TS-1 samples prepared by deposition-precipitation method (Au/TS-1 (DP)), b) UV-Vis spectrum, d) and f) XPS-spectra of fresh (calcined) and thermally treated (873 K, 18 h) Au encapsulated in macroporous TS-1 (Au/MTS- 1) samples.

Catalytic properties

To study the activity and the accessibility of both the gold and the titanium sites in the bifunctional hierarchical zeolites, we tested a sample of Au/MTS-1 for the direct epoxidation of propene with hydrogen and oxygen. The bifunctional catalysts for the reaction need gold sites to form peroxy species and

titanium sites for the epoxidation reaction.[21k] Catalysts that only contain one of the functions (gold or titanium sites) are not active for the direct epoxidation reaction. Further, the very active bifunctional catalysts based on gold supported on TS-1, suffer from sintering of the gold particles, even under the mild reaction conditions.[29]

For the catalytic evaluation, a sample of macroporous TS-1 (Si/Ti = 40) with 0.5 wt% of encapsulated gold was synthesised, calcined and treated under hydrogen before reaction. Detailed characterisation data can be found in the electronic supporting information.

The propene conversion and selectivity to propylene oxide as well as the production rate of different oxygenates as a function of reaction temperature are shown in Figure 7.

The propene conversion increases with reaction temperature and reaches values comparable to other bifunctional gold/TS-1 catalysts.[29] The formation of propylene oxide increases with reactor temperature. Beside PO, other oxygenates are produced in large quantities, the biggest fraction being propanal. The formation of these oxygenates increases with reaction temperature too. Furthermore, the increase with temperature is more pronounced for the formation of oxygenates than for PO formation. Due to this formation of oxygenates, the selectivity to propylene oxide (PO) decreases with the reaction temperature.

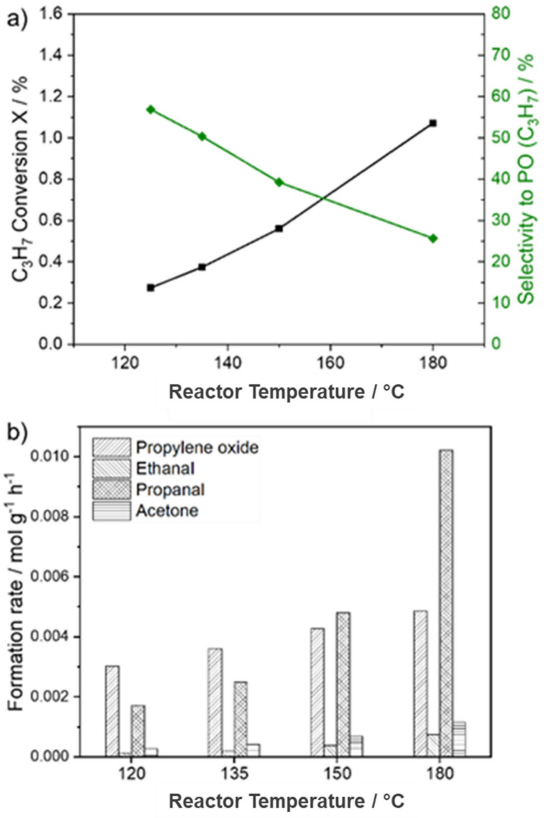

Figure 7. a) Propene conversion and propylene oxide selectivity and b) product formation rate as a function of internal reactor temperature for epoxidation of propene with oxygen and hydrogen. Catalyst: Au/MTS-1 (0.5 wt.-% Au, Si/Ti = 40). Formation rate per gram of catalyst without SiC.

The catalytic results show that the tested Au/MTS-1 catalyst is active for the direct epoxidation of propene to propylene oxide and, subsequently, both active sites (Au and framework Ti sites) are active and accessible. However, while the activity is comparable to conventional Au/TS-1 catalysts, the selectivity to PO is not. The catalyst produces rather large amounts of oxygenates, mainly acetone, as well as water and CO_2.

This could indicate an imbalance in terms of activity of the different active sites or suboptimal proximity between Au and Ti sites. The two main steps of the assumed reaction mechanism for direct propene epoxidation are the reaction of hydrogen and oxygen on the gold sites to form peroxide species and the formation of propoxy species by adsorption of propene on Ti sites. Both species then react and form propene oxide.[25] If the active sites are present in the wrong ratio or not in close proximity, the formation of oxygenates is possible. The formation of peroxide species on the Au particles is usually the rate determining step and, thus, no peroxide species could be observed. *In situ* studies using IR and Raman spectroscopy might help to better understand the activity of both active sites, as the observation of peroxide species in such measurements would indicate an activity imbalance. Future catalyst optimisation could balance the activity of the two different active sites, to create not only a more active and stable, but also more selective epoxidation catalyst.

Conclusion

A flexible procedure was proposed for the one-pot synthesis of hierarchically structured zeolites with encapsulated noble metal particles. Both the noble metal and the heteroatoms can be changed, allowing for numerous different combinations of active sites, and making the proposed materials synthesis method highly versatile. The synthesised samples have a high crystallinity and micropore volume and an interconnected network of evenly distributed intracrystalline macropores with diameters between about 200 and 500 nm.

The synthesised materials show remarkable sinter resistance. No significant sintering of the encapsulated gold, platinum and palladium particles was observed during the harsh calcination of the samples at 823 K for 6 h, presenting clear evidence for successful encapsulation within the zeolite. Additional investigations showed that the encapsulation of Au nanoparticles within the hierarchical zeolites effectively prevents their sintering, even during treatment at high temperature for a long period (873 K, 18 h) which led to significant sintering in a conventional Au/TS-1 sample.

Catalytic studies for propene epoxidation could further show that both catalytic functions in an Au/TS-1 sample, tetrahedral Ti sites and Au nanoparticles, are active and accessible. However, the catalyst still needs to be optimised in terms of balancing both catalytic functions to archive higher PO selectivity, a subject beyond the scope of this material focused article. Then investigations on the long-term stability and sintering under reaction conditions of the Au/TS-1 samples would be very interesting.

We believe that the presented material, combining the advantages of noble metal encapsulation with a hierarchical pore system, has great potential for many different reactions, due to its high resistance against sintering, short diffusion path length, and small, encapsulated metal nanoparticles. Furthermore, the one-pot synthesis approach is relatively simple and very flexible, allowing encapsulation of different metals, incorporation of different heteroatoms in the zeolite framework and good control over the macropore system.

Experimental Section

Synthesis of mesoporous silica particles

Spherical mesoporous silica particles (MSPs) were used as substrate for the preparation of macroporous zeolites. The MSPs were synthesised using the procedure reported by Machoke et al.[15a,26] A detailed description of the MSPs synthesis can be found in the supporting information.

Synthesis of macroporous zeolites with encapsulated noble metal

The synthesis of macroporous zeolites with encapsulated metal nanoparticles was based on previously reported synthesis procedures for silicalite-1, ZSM-5 and TS-1.[15b,c] The corresponding macroporous, hierarchically structured samples of the latter are called MZSM-5 and MTS-1. Silicalite-1 is the Al-free form of ZSM-5.

The preparation consists of the following steps: Synthesis of MSPs, wetness impregnation of MSPs with the heteroatom source, and subsequent incipient wetness impregnation of the heteroatom-containing MSPs with the structure-directing agent and the mercaptosilane-stabilised noble metal precursor. This is followed by steam-assisted crystallisation of the impregnated and dried MSPs to form the macroporous zeolite.

Synthesis of noble metal containing, macroporous ZSM-5

In a typical synthesis, 1 g of calcined MSPs was added to 3.15 g of a 2 wt% $Al(NO_3)_3.9\ H_2O$ solution, mixed with a spatula and then dried at 303 K for 3 h.

All syntheses were carried out by using a molar ratio of 3-mercaptopropyl-trimethoxysilane to noble metal precursor of 6. The calculated amount of 3-mercaptopropyl-trimethoxysilane (95%, Sigma-Aldrich) was dissolved in 1.4 g TPAOH solution (40 wt%, Sigma-Aldrich) and stirred for 16 h. The necessary amount of the noble metal precursor was dissolved in 0.4 g of deionised (DI) water and then added dropwise to the TPAOH and 3-mercaptopropyl-trimethoxysilane solution. The resulting mixture (Mixture A) was stirred for 2 h. The Al-impregnated, dried MSPs were subsequently impregnated with mixture A, stirred with a spatula, and then dried at 313 K for 1.5 h in a convection oven. The dried impregnated MSPs were crushed into a fine powder and distributed into cylindrical PTFE crucibles with a volume of 5 ml. The crucibles were placed on top of spacer tubes in 23 ml PTFE-lined stainless-steel autoclaves (Parr) filled with 4.0 g DI water. Steam-assisted crystallisation was carried out at 403 K for 48 h. After crystallisation, the solid products were recovered by centrifugation, washed with a water/ethanol mixture, and dried at 348 K for 16 h. To remove the structure directing agent, the samples were calcined in a muffle furnace under 300 l h^{-1} air flow at 823 K (heating ramp 1.2 K min^{-1}). Reduction treatments were carried out in a tubular furnace at 673 K for 2 hours under diluted hydrogen flow (10 ml min^{-1} H_2 and 90 ml min^{-1} N_2).

The calcined samples were then transferred into the ammonium form by three-fold ion exchange with 1.0 M aqueous ammonium nitrate (Merck Emsure) solution at 338 K for 6 h ($w_{liquid}/w_{solid} = 30$). The samples were then converted into the proton form by calcination in a muffle furnace under 300 l h^{-1} air flow at 823 K for 4 h (heating ramp 1.2 K min^{-1}).

Synthesis of noble metal containing macroporous TS-1

In a typical synthesis, 1.0 g of calcined MSPs was added into 1.9 g of a 5.0 wt% titanium butoxide solution in isopropanol, mixed with a spatula and then dried at 303 K for 3 h. The dry powder was stored at room temperature overnight and then impregnated with a mixture of organic structure directing agent (OSDA) and stabilised noble metal precursor (Mixture A, see before). Afterwards, the impregnated MSPs were dried at 313 K for 1.5 h in a convection oven. Zeolite synthesis by steam-assisted crystallisation was carried out as described before for macroporous ZSM-5, however, the temperature was increased to 423 K and the duration to 72 h. Sample separation and calcination were carried out as for the aforementioned ZSM-5 samples.

Synthesis of the reference Au supported on TS-1 zeolite

Conventional TS-1 was synthesised according to the procedure reported by Nijhuis et al.[27] Gold was supported on this conventional TS-1 sample by the deposition precipitation method, following a procedure reported in the literature.[27–28] Due to light sensitivity, the catalyst was prepared in the dark, in amber coloured glassware. Typically, 1.32 g calcined TS-1 was dispersed in 100 ml DI water and the pH was adjusted to 9–10 by adding a diluted, aqueous ammonia solution (2.5 wt%, Merck). Then 0.0228 g of chloroauric acid trihydrate ($HAuCl_4.3H_2O$), dissolved in 20 ml of DI water, was added dropwise while maintaining the pH at around 9.5, to achieve a gold loading of 1 wt.-% The solid was recovered by centrifugation, washed with DI water and dried at 353 K for 16 h, followed by calcination at 673 K for 4 h (heating ramp 5 K min^{-1}).

Catalytic investigation for direct epoxidation of propene

The direct gas phase epoxidation of propene was carried out in a fixed, packed bed, quartz glass reactor with an inner diameter of 9 mm and a K-type probe thermocouple. 0.5 g of catalyst was mixed with 2.5 g of silicon carbide. The reaction feed consisted of 10/10/10/70 vol% of $C_3H_6/H_2/O_2$/He, respectively, with a total flow rate of 66.7 ml min^{-1}, resulting in a gas hourly space velocity (GHSV) of 8000 ml g_{cat}^{-1} h^{-1}. The reactor outlet gas was analysed by online gas chromatography (GC, Shimadzu). The oxygenates (PO, ethanal, propanal, acetone and acrolein), along with CO_2, H_2O and C_3H_6, were separated using a Porapak T column and analysed by a flame ionisation detector (FID), while the permanent gases (H_2, O_2, CO) were separated by a Molsieve 5 A column and analysed by a thermal conductivity detector (TCD). More details can be found in our previous work.[29]

Characterisation

Powder XRD patterns were measured from 2 to 55° (2θ with a Stoe STADI P diffractometer equipped with a Cu Kα1 source using 0.5 mm borosilicate glass capillaries. N_2 adsorption and desorption isotherms were measured using a Quantachrome Quadrasorb at

77 K. Prior to measurement, all samples were degassed for 12 h under vacuum at 525 K. The elemental composition was measured using microwave plasma - atomic emission spectrometry. Samples were dissolved by flux melting at 1323 K, using sodium tetraborate as flux in a 1:10 mass ratio using a Pt crucible. The molten sample was dissolved in *aqua regia* and diluted before the measurement. Microwave plasma-atomic emission spectrometer measurements were carried out using an Agilent 4100 MP-AES instrument. X-ray photoelectron spectroscopy (XPS) measurements were conducted using 150 scans per element with 20 eV pass energy. Casa XPS software was used for data processing. The peak area ratio of the Au 4f doublet ($f_{5/2}$:$f_{7/2}$) was fixed to 3:4. Transmission electron microscopy (TEM) images were obtained using a JEOL 2100 microscope operating at 200 kV. Samples were dispersed in ethanol and then drop-casted onto holey carbon-coated copper grids (EM Resolutions).

Acknowledgements

Funding from the EPSRC via a "Frontier Engineering" and "Frontier Engineering: Progression" Awards (EP/K038656/1, EP/S03305X/1) is gratefully acknowledged. We thank Halan Mohamed for her help with the XPS measurements.

Conflict of Interest

The authors declare no conflict of interest.

Data Availability Statement

The data that support the findings of this study are available from the corresponding author upon reasonable request.

Keywords: bifunctional catalysis · catalysis · encapsulation · sintering · zeolite

[1] a) S.-M. Wu, X.-Y. Yang, C. Janiak, *Angew. Chem. Int. Ed.* **2019**, *58*, 12340–12354; *Angew. Chem.* **2019**, *131*, 12468–12482; b) X. Li, X. Hao, A. Abudula, G. Guan, *J. Mater. Chem. A* **2016**, *4*, 11973–12000; c) D. Pakhare, J. Spivey, *Chem. Soc. Rev.* **2014**, *43*, 7813–7837; d) J. Li, T. Zhao, T. Chen, Y. Liu, C. N. Ong, J. Xie, *Nanoscale* **2015**, *7*, 7502–7519; e) S. Guo, E. Wang, *Nano Today* **2011**, *6*, 240–264.

[2] a) R. Jin, C. Zeng, M. Zhou, Y. Chen, *Chem. Rev.* **2016**, *116*, 10346–10413; b) A. Wang, J. Li, T. Zhang, *Nat. Chem. Rev.* **2018**, *2*, 65–81; c) I. Chakraborty, T. Pradeep, *Chem. Rev.* **2017**, *117*, 8208–8271; d) H. Song, F. Kim, S. Connor, G. A. Somorjai, P. Yang, *J. Phys. Chem. B* **2005**, *109*, 188–193; e) Y. Zhang, X. Cui, F. Shi, Y. Deng, *Chem. Rev.* **2012**, *112*, 2467–2505.

[3] a) F. Rodríguez-Reinoso, A. Sepúlveda-Escribano, *Carbon materials for catalysis* **2009**, 131–155; b) B. L. Mojet, M. J. Kappers, J. T. Miller, D. C. Koningsberger, in *Studies in Surface Science and Catalysis, Vol. 101* (Eds.: J. W. Hightower, W. Nicholas Delgass, E. Iglesia, A. T. Bell), Elsevier, **1996**, pp. 1165–1174; c) B. A. Mehrabadi, S. Eskandari, U. Khan, R. D. White, J. R. Regalbuto, in *Advances in Catalysis, Vol. 61*, Elsevier, **2017**, pp. 1–35; d) W. E. Kaden, T. Wu, W. A. Kunkel, S. L. Anderson, *Science* **2009**, *326*, 826–829.

[4] a) C. H. Bartholomew, *Appl. Catal. A* **2001**, *212*, 17–60; b) A. Cao, R. Lu, G. Veser, *Phys. Chem. Chem. Phys.* **2010**, *12*, 13499–13510; c) G. M. Veith, A. R. Lupini, S. Rashkeev, S. J. Pennycook, D. R. Mullins, V. Schwartz, C. A. Bridges, N. J. Dudney, *J. Catal.* **2009**, *262*, 92–101; d) F. Yang, M. S. Chen, D. W. Goodman, *J. Phys. Chem. C* **2009**, *113*, 254–260; e) P. Forzatti, L. Lietti, *Catal. Today* **1999**, *52*, 165–181.

[5] C. T. Campbell, S. C. Parker, D. E. Starr, *Science* **2002**, *298*, 811–814.

[6] a) P. M. Arnal, M. Comotti, F. Schüth, *Angew. Chem. Int. Ed.* **2006**, *45*, 8224–8227; *Angew. Chem.* **2006**, *118*, 8404–8407; b) J. Mielby, J. O. Abildstrøm, F. Wang, T. Kasama, C. Weidenthaler, S. Kegnæs, *Angew. Chem. Int. Ed.* **2014**, *53*, 12513–12516; *Angew. Chem.* **2014**, *126*, 12721–12724.

[7] M. T. Bore, H. N. Pham, T. L. Ward, A. K. Datye, *Chem. Commun.* **2004**, *22*, 2620–2621.

[8] a) L. Liu, M. Lopez-Haro, C. W. Lopes, C. Li, P. Concepcion, L. Simonelli, J. J. Calvino, A. Corma, *Nat. Mater.* **2019**, *18*, 866–873; b) J. Zhang, L. Wang, B. Zhang, H. Zhao, U. Kolb, Y. Zhu, L. Liu, Y. Han, G. Wang, C. Wang, D. S. Su, B. C. Gates, F.-S. Xiao, *Nature Catalysis* **2018**, *1*, 540–546.

[9] a) B. Wichtelova, Z. Sobalik, J. Dedecek, *Appl. Catal. B* **2003**, *41*, 97–114; b) D. BARTHOMEUF , *Catal. Rev.* **1996**, *38*, 521–612; c) N. Katada, K. Suzuki, T. Noda, G. Sastre, M. Niwa, *J. Phys. Chem. C* **2009**, *113*, 19208–19217.

[10] a) D. Farrusseng, A. Tuel, *New J. Chem.* **2016**, *40*, 3933–3949; b) M. J. Climent, A. Corma, S. Iborra, M. J. Sabater, ACS Publications, **2014**; c) D. Jagadeesan, *Appl. Catal. A* **2016**, *511*, 59–77; d) H. J. Cho, D. Kim, J. Li, D. Su, B. Xu, *J. Am. Chem. Soc.* **2018**, *140*, 13514–13520.

[11] a) T.-L. Cui, W.-Y. Ke, W.-B. Zhang, H.-H. Wang, X.-H. Li, J.-S. Chen, *Angew. Chem. Int. Ed.* **2016**, *55*, 9178–9182; *Angew. Chem.* **2016**, *128*, 9324–9328; b) C. Wang, E. Guan, L. Wang, X. Chu, Z. Wu, J. Zhang, Z. Yang, Y. Jiang, L. Zhang, X. Meng, B. C. Gates, F.-S. Xiao, *J. Am. Chem. Soc.* **2019**, *141*, 8482–8488; c) S. Altwasser, R. Gläser, J. Weitkamp, *Microporous Mesoporous Mater.* **2007**, *104*, 281–288.

[12] S. Li, T. Boucheron, A. Tuel, D. Farrusseng, F. Meunier, *Chem. Commun.* **2014**, *50*, 1824–1826.

[13] a) J. Kärger, D. Freude, *Chem. Eng. Technol.* **2002**, *25*, 769–778; b) P. Zeigermann, J. Kärger, R. Valiullin, *Microporous Mesoporous Mater.* **2013**, *178*, 84–89.

[14] a) J. Pérez-Ramírez, C. H. Christensen, K. Egeblad, C. H. Christensen, J. C. Groen, *Chem. Soc. Rev.* **2008**, *37*, 2530–2542; b) W. Schwieger, A. G. Machoke, T. Weissenberger, A. Inayat, T. Selvam, M. Klumpp, A. Inayat, *Chem. Soc. Rev.* **2016**, *45*, 3353–3376; c) M. O. Coppens, T. Weissenberger, Q. Zhang, G. Ye, *Adv. Mater. Interfaces* **2020**, *8*, 2001409.

[15] a) A. G. Machoke, A. M. Beltrán, A. Inayat, B. Winter, T. Weissenberger, N. Kruse, R. Güttel, E. Spiecker, W. Schwieger, *Adv. Mater.* **2015**, *27*, 1066–1070; b) T. Weissenberger, R. Leonhardt, B. A. Zubiri, M. Pitínová-Štekrová, T. L. Sheppard, B. Reiprich, J. Bauer, R. Dotzel, M. Kahnt, A. Schropp, C. G. Schroer, J.-D. Grunwaldt, J. L. Casci, J. Čejka, E. Spiecker, W. Schwieger, *Chem. Eur. J.* **2019**, *25*, 14430–14440; c) T. Weissenberger, B. Reiprich, A. G. F. Machoke, K. Klühspies, J. Bauer, R. Dotzel, J. L. Casci, W. Schwieger, *Catalysis Science, Technology* **2019**, *9*, 3259–3269.

[16] M. Choi, Z. Wu, E. Iglesia, *J. Am. Chem. Soc.* **2010**, *132*, 9129–9137.

[17] a) B. Apeleo Zubiri, J. Wirth, D. Drobek, S. Englisch, T. Przybilla, T. Weissenberger, W. Schwieger, E. Spiecker, *Adv. Mater. Interfaces* **2020**, *8*, 2001154; b) T. Weissenberger, A. G. F. Machoke, B. Reiprich, W. Schwieger, *Advanced Materials Interfaces* **2020**, *8*, 2001653.

[18] Z. Guo, X. Li, S. Hu, G. Ye, X. Zhou, M. O. Coppens, *Angew. Chem.* **2020**, *132*, 1564–1567; *Angew. Chem. Int. Ed.* **2020**, *59*, 1548–1551.

[19] a) T. Blasco, M. Camblor, A. Corma, J. Perez-Pariente, *J. Am. Chem. Soc.* **1993**, *115*, 11806–11813; b) F. Geobaldo, S. Bordiga, A. Zecchina, E. Giamello, G. Leofanti, G. Petrini, *Catal. Lett.* **1992**, *16*, 109–115; c) P. Wu, T. Tatsumi, T. Komatsu, T. Yashima, *J. Phys. Chem. B* **2001**, *105*, 2897–2905.

[20] V. Amendola, M. Meneghetti, *J. Phys. Chem. C* **2009**, *113*, 4277–4285.

[21] a) D. P. Anderson, R. H. Adnan, J. F. Alvino, O. Shipper, B. Donoeva, J.-Y. Ruzicka, H. Al Qahtani, H. H. Harris, B. Cowie, J. B. Aitken, V. B. Golovko, G. F. Metha, G. G. Andersson, *Phys. Chem. Chem. Phys.* **2013**, *15*, 14806–14813; b) D. P. Anderson, J. F. Alvino, A. Gentleman, H. A. Qahtani, L. Thomsen, M. I. J. Polson, G. F. Metha, V. B. Golovko, G. G. Andersson, *Phys. Chem. Chem. Phys.* **2013**, *15*, 3917–3929; c) C. Battistoni, G. Mattogno, F. Cariati, L. Naldini, A. Sgamellotti, *Inorg. Chim. Acta* **1977**, *24*, 207–210; d) V. D. Borman, M. A. Pushkin, V. N. Tronin, V. I. Troyan, *J. Exp. Theor. Phys.* **2010**, *110*, 1005–1025; e) B. Chowdhury, K. K. Bando, J. J. Bravo-Suárez, S. Tsubota, M. Haruta, *J. Mol. Catal. A* **2012**, *359*, 21–27; f) C. C. Chusuei, X. Lai, K. A. Davis, E. K. Bowers, J. P. Fackler, D. W. Goodman, *Langmuir* **2001**, *17*, 4113–4117; g) B. G. Donoeva, D. S. Ovoshchnikov, V. B. Golovko, *ACS Catal.* **2013**, *3*, 2986–2991; h) Y. Kitsudo, A. Iwamoto, H. Matsumoto, K. Mitsuhara, T. Nishimura, M. Takizawa, T. Akita, Y. Maeda, Y. Kido, *Surf. Sci.* **2009**, *603*, 2108–2114; i) A. Y. Klyushin, T. C. R. Rocha, M. Hävecker, A. Knop-Gericke, R. Schlögl,

Phys. Chem. Chem. Phys. **2014**, *16*, 7881–7886; j) J.-Y. Ruzicka, F. Abu Bakar, C. Hoeck, R. Adnan, C. McNicoll, T. Kemmitt, B. C. Cowie, G. F. Metha, G. G. Andersson, V. B. Golovko, *J. Phys. Chem. C* **2015**, *119*, 24465–24474; k) Y. Yuan, K. Asakura, A. P. Kozlova, H. Wan, K. Tsai, Y. Iwasawa, *Catal. Today* **1998**, *44*, 333–342.

[22] a) Z. Ebrahimpour, N. Mansour, *Appl. Surf. Sci.* **2017**, *394*, 240–247; b) Z. Jiang, W. Zhang, L. Jin, X. Yang, F. Xu, J. Zhu, W. Huang, *J. Phys. Chem. C* **2007**, *111*, 12434–12439; c) S. Saris, V. Niemann, V. Mantella, A. Loiudice, R. Buonsanti, *Nanoscale* **2019**, *11*, 19543–19550; d) C. Tan, Y. Sun, J. Zheng, D. Wang, Z. Li, H. Zeng, J. Guo, L. Jing, L. Jiang, *Sci. Rep.* **2017**, *7*, 6347; e) M. Xue, Y. Tan, *Nanoscale* **2014**, *6*, 12500–12514.

[23] a) N. Kruse, S. Chenakin, *Appl. Catal. A* **2011**, *391*, 367–376; b) S. Arrii, F. Morfin, A. J. Renouprez, J. L. Rousset, *J. Am. Chem. Soc.* **2004**, *126*, 1199–1205.

[24] a) K. Okazaki, S. Ichikawa, Y. Maeda, M. Haruta, M. Kohyama, *Appl. Catal. A* **2005**, *291*, 45–54; b) A. Vijay, G. Mills, H. Metiu, *J. Chem. Phys.* **2003**, *118*, 6536–6551.

[25] T. A. Nijhuis, B. M. Weckhuysen, *Catal. Today* **2006**, *117*, 84–89.

[26] T. Weissenberger, A. G. F. Machoke, J. M. Kolle, Y. S. Avadhut, M. Hartmann, W. Schwieger, *Chem. Ing. Tech.* **2021**, *93*, 1001–1010.

[27] T. A. Nijhuis, B. J. Huizinga, M. Makkee, J. A. Moulijn, *Ind. Eng. Chem. Res.* **1999**, *38*, 884–891.

[28] J. Chen, S. J. Halin, E. A. Pidko, M. Verhoeven, D. M. P. Ferrandez, E. J. Hensen, J. C. Schouten, T. A. Nijhuis, *ChemCatChem* **2013**, *5*, 467–478.

[29] N. Kapil, T. Weissenberger, F. Cardinale, P. Trogadas, T. A. Nijhuis, M. M. Nigra, M.-O. Coppens, *Angew. Chem. Int. Ed.* **2021**, *60*, 18185–18193.

Manuscript received: February 23, 2022
Revised manuscript received: April 26, 2022
Accepted manuscript online: April 27, 2022
Version of record online: ■■, ■■■

RESEARCH ARTICLE

Metal nanoparticles encapsulated in hierarchical, micro/macroporous zeolites were synthesised by crystallisation of mesoporous silica particles impregnated with stabilised metal precursors. The encapsulation proved to be very effective in preventing the sintering of the metal particles even at high temperatures. Catalytic tests showed that the encapsulated metal particles remained accessible and active.

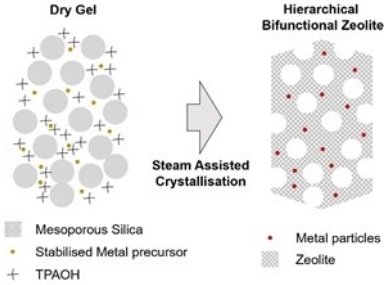

Dr. T. Weissenberger, Dr. N. Kapil, Dr. P. Trogadas, Prof. M.-O. Coppens**

1 – 10

One-pot Synthesis of Hierarchical, Micro-macroporous Zeolites with Encapsulated Metal Particles as Sinter-resistant, Bifunctional Catalysts